HYDROLOGICAL PROCESSES
Hydrol. Process. **22**, 4877–4891 (2008)
Published online 10 September 2008 in Wiley InterScience
(www.interscience.wiley.com) DOI: 10.1002/hyp.7107

River flow forecasting using wavelet and cross-wavelet transform models

Jan F. Adamowski*
Cyprus Institute Program for Energy, Environment, and Water Resources, Massachusetts Institute of Technology, 77 Massachusetts Avenue, E40-476, Cambridge, MA 02139, USA

Abstract:

In this study, short-term river flood forecasting models based on wavelet and cross-wavelet constituent components were developed and evaluated for forecasting daily stream flows with lead times equal to 1, 3, and 7 days. These wavelet and cross-wavelet models were compared with artificial neural network models and simple perseverance models. This was done using data from the Skrwa Prawa River watershed in Poland. Numerical analysis was performed on daily maximum stream flow data from the Parzen station and on meteorological data from the Plock weather station in Poland. Data from 1951 to 1979 was used to train the models while data from 1980 to 1983 was used to test the models. The study showed that forecasting models based on wavelet and cross-wavelet constituent components can be used with great accuracy as a stand-alone forecasting method for 1 and 3 days lead time river flood forecasting, assuming that there are no significant trends in the amplitude for the same Julian day year-to-year, and that there is a relatively stable phase shift between the flow and meteorological time series. It was also shown that forecasting models based on wavelet and cross-wavelet constituent components for forecasting river floods are not accurate for longer lead time forecasting such as 7 days, with the artificial neural network models providing more accurate results. Copyright © 2008 John Wiley & Sons, Ltd.

KEY WORDS forecasting; wavelet transform; floods

Received 17 March 2007; Accepted 23 May 2008

INTRODUCTION

The accuracy of models used for any flood forecasting and warning system is critical since an accurate flood forecast with sufficient lead time can provide advanced warning of an impending flood at an early enough stage such that flood damage can be reduced significantly. The importance of an accurate flow forecast, especially in flood-prone areas, has increased significantly over the last few years as extreme events have become more frequent and more severe due to climate change and anthropogenic factors.

Data-based forecasting methods are becoming increasingly popular in flood forecasting applications due to their rapid development times, minimum information requirements, and ease of real-time implementation. In data-based flood forecasting, statistical models have traditionally been used, such as multiple linear regression, autoregressive moving average, and artificial neural network models. However, a problem with these and other linear and non-linear methods is that they have limitations with non-stationary data. In the last decade, wavelet analysis has been investigated in a number of disciplines outside of hydrology, and it has been found to be very effective with non-stationary data. However, the use of wavelet analysis as a stand-alone flood forecasting method has not been explored in great detail in the literature, and this constituted the main purpose of this research.

* Correspondence to: Jan F. Adamowski, 214 Goulburn Ave., Ottawa, Canada, K1N 8E4, Tel/Fax: 613 565 6146. E-mail: adamowsk@mit.edu

PREVIOUS RESEARCH

Many applications of artificial neural networks can be found in the hydrological literature (Kang *et al.*, 1993; Hsu *et al.*, 1995; Kim and Barros, 2001; Tawfik, 2003; Nayak *et al.*, 2005; and Piotrkowski *et al.*, 2006 among others).

Wavelets, due to their attractive properties, have been explored for use in time series analysis. Wavelet transforms provide useful decompositions of original time series, so that wavelet-transformed data improves the ability of a forecasting model by capturing useful information on various resolution levels. In the field of hydrology, wavelet analysis has recently been applied to examine the rainfall–runoff relationship in a Karstic watershed (Labat *et al.*, 1999), to characterize daily streamflow (Smith *et al.*, 1998; Saco and Kumar, 2000) and monthly reservoir inflow (Coulibaly *et al.*, 2000), and to evaluate rainfall–runoff models (Lane, 2007). Several studies have been published that developed hybrid wavelet–ANN models. Wang and Lee (1998) developed a hybrid wavelet–ANN model to forecast rainfall–runoff in China, Kim *et al.* (2003) developed a similar model to forecast droughts in Mexico, and Cannas *et al.* (2005) developed a hybrid model for monthly rainfall–runoff forecasting in Italy. Each of these studies found that the ANNs trained with the pre-processed data had better performance than the ANNs trained with undecomposed time series data, although the differences were small. Tantanee *et al.* (2005) developed a coupled wavelet–autoregressive model for annual rainfall prediction.

STUDY SITE AND DATA

Skrwa Prawa River watershed description

The Skrwa Prawa River is the largest right-bank inflow to the Vistula River in the north-west region of Mazowsze in Poland. The Skrwa Prawa River is 114 km in length and has a watershed area of 1534 km^2. Floods in the Skawa Prawa River are almost always of snowmelt origin and occur between January and June. As such, wavelet flood forecasting models were developed for each day between 1 January and 30 June.

Skrwa Prawa River data description

The daily stream flow data (maximum daily flow in m^3 s^{-1}) was taken for the Skrwa Prawa River in Poland from the Parzen streamflow gauge station. The daily streamflow series record starts in 1951 and ends in 1983. The data was divided into training and testing data sets. The former set began in 1951 and ended in 1979 while the testing set began in 1980 and ended in 1983. During this period, the minimum flow was 0·50 m^3 s^{-1}, the maximum flow was 191·00 m^3 s^{-1}, and the average flow was 6·49 m^3 s^{-1}.

The daily meteorological data was taken from the weather station in Plock, Poland, which is very close to the Parzen streamflow gauge station. The daily record of the meteorological series data starts in 1951 and continues to 1983, including the maximum temperature (°C) reached at the location for that day, the minimum temperature (°C) reached at the location for that day, the total amount of atmospheric precipitation (mm), and the depth of snow (cm) on the ground. As with the streamflow data, the meteorological data was divided into training and testing data sets. The former set began in 1951 and ended in 1979 while the testing set began in 1980 and ended in 1983.

For both the flow (F) and meteorological (precipitation P, minimum temperature TI, and maximum temperature TA) data, data from the entire year for each year from 1951 to 1979 was used for the training phase, while data from only 1 January to 30 June for each year from 1980 to 1983 was used for the testing phase. As such, data from each day of the entire year for all training years was used for the training of the models. This was done in order to assess whether *not* artificially splitting the data in the training phase would result in accurate forecasting models for the 1 January to 30 June testing period. In wavelet analysis, splitting the data artificially can result in potentially very significant edge effect errors in terms of the amplitude and phase discontinuity biases. This was found to be the case in the preliminary analysis of the Skrwa Prawa flow and meteorological data. Thus, it was decided to assess the forecasting ability of models developed from training data that was not split artificially, but tested for the January to June period only. Due to the fact that the wavelet forecasting models are based on daily constituent components consisting of different daily values, and because the models take into account the daily non–stationary nature of the data, it was assumed that not artificially splitting the data would not pose any significant problems in terms of the resulting constituent components.

THEORETICAL BACKGROUND

Wavelet transform

The Morlet–Grossmann definition (Grossmann and Morlet, 1984) of the continuous wavelet transform is:

$$W(s,n) = \frac{1}{\sqrt{s}} \int_{-\infty}^{+\infty} x_n, \psi^* \left(\frac{n'-n}{s}\right) dn' \qquad (1)$$

where $W(s,n)$ is the wavelet coefficient of the time series $x_{n'}$, ψ is the analysing wavelet (which is the Morlet wavelet in this study), s (>0) is the scale, n is the translation, and n' is the location (or time). Scale is the width of the wavelet: a larger scale means that more of the time series is included in the calculation and that finer details are ignored. A wavelet of varying width (scale) is translated (moved) through the entire time series. The wavelet transformation is therefore localized in both time (through the translation) and frequency (through the range of scales).

There are a variety of wavelet functions that can be used. In order to be admissible as a wavelet, this function must have zero mean and be localized in both time and frequency space. In this study, the complex non-orthogonal Morlet wavelet function was used, which can be used for signals with strong wave-like features (which is the case with streamflow data). The Morlet wavelet is a sinusoid with wavelength s modulated by a Gaussian function, and has provided robust results in analyses of time series records (Appenzeller *et al.*, 1998; Gedalof and Smith, 2001). The parameter l is used to modify wavelet transform bandwidth-resolution either in favour of time or in favour of frequency, and represents the length of the mother wavelet or analysis window.

The shifted and scaled Morlet mother wavelet can be defined as (Morlet *et al.*, 1982):

$$\psi_{s,n'}^{l}(n) = \pi^{-1/4}(sl)^{-1/2}e^{-i2\pi\frac{1}{s}(n-n')}e^{-\frac{1}{2}(\frac{n-n'}{sl})^2} \qquad (2)$$

Cross-wavelet transform

When comparing two different variables like temperature or flow, or when analysing tele-connections, one needs the bivariate extension of wavelet analysis. Cross-wavelet analysis was introduced by, among others, Hudgins *et al.* (1993). In hydrology, it has been used, for example, in rainfall–runoff cross-analysis (Labat *et al.*,

DOI: 10.1002/hyp

1999). In this research, cross-wavelet analysis was used to determine the phase difference $\Delta\phi_{n',s}$ values between the flow and meteorological variables, and to develop cross-wavelet constituent components. The phase difference (shift) between variables x and y is defined by (Jury *et al.*, 2002):

$$\Delta\phi_{x,y,n',s} = \tan^{-1}\frac{\int_{s1}^{s2} Im(W_{x,y,n',s})ds}{\int_{s1}^{s2} \mathrm{Re}(W_{x,y,n',s})ds} \tag{3}$$

where Im and Re indicate the imaginary and real part, respectively. The cross-amplitude of variables x and y is defined by (Jury *et al.*, 2002):

$$W_{x,y,n',s} = W_{x,n',s}W_{y,n',s} \tag{4}$$

Equation (4) has the advantage that s is used unambiguously for both variables, resulting in very precise calibrations. For flow components, there is no $\Delta\phi_{n',s}$ term.

Model performance comparison

The performance of a model can be measured by the root mean square error (RMSE), the coefficient of determination (R^2), and the efficiency index (EI).

The root mean square error evaluates the variance of errors independently of the sample size, and is given by:

$$RMSE = \sqrt{\frac{SEE}{N}} \tag{5}$$

where SEE is the sum of squared errors, and N is the number of data points used. SEE is given by:

$$SEE = \sum_{i=1}^{N}(y_i - \hat{y}_i)^2 \tag{6}$$

where y_i is the observed flow, and $\hat{y}_i$ is the computed flow from the model. The smaller the RMSE, the better the performance of the model.

The coefficient of determination (R^2) measures the degree of correlation among the observed and predicted values. It is a measure of the strength of the model in developing a relationship among input and output variables. The higher the R^2 value (with 1 being the maximum value), the better is the performance of the model. R^2 is given by:

$$R^2 = \frac{\sum_{i=1}^{N}(\hat{y}_i - \overline{y}_i)^2}{\sum_{i=1}^{N}(y_i - \overline{y}_i)^2} \tag{7}$$

and

$$\overline{y}_i = \frac{1}{N}\sum_{i=1}^{N} y_i \tag{8}$$

where $\overline{y}_i$ is the mean value taken over N, with the other variables having already been defined.

As a measure of accuracy, one can use the efficiency index (EI), which measures the agreement between simulated and actual values of a given parameter as a proportion of the total range of that parameter in the data. The value of the EI ranges from a maximum value of one to a minimum of minus infinity. The higher the value of the EI, the better is the performance of the model. It is given by (Nash and Sutcliffe, 1970):

$$EI = 1 - \frac{SE}{ST} \tag{9}$$

where SE is the sum square of errors given by:

$$SE = \sum_{i=1}^{N}(y_i - \hat{y}_i)^2 \tag{10}$$

and ST is the total variation given by:

$$ST = \sum_{i=1}^{N}(y_i - \overline{y})^2 \tag{11}$$

MODEL DEVELOPMENT

Artificial neural network analysis

Back propagation feedforward ANNs with the 'generalized delta rule' (BP–MLP) as the training algorithm, were used to develop all the ANN models. The Tiberius 2·0·0 neural network modeling software package was used for the ANN analysis. To develop an ANN model, the primary objective is to arrive at the optimum architecture of the ANN that captures the relationship between the input and output variables. In this study, ANN networks consisting of an input layer with 1 to 8 input nodes, one single hidden layer composed of 4 to 7 nodes (1 to 8 were tested), and one output layer consisting of one node denoting the forecasted stream flow were developed. The optimum learning coefficients were found to be between 0·03 and 0·05 for the ANN models.

The inputs of each model consisted of all or some of the following variables: maximum temperature of the current day $T_{\max}$, minimum temperature of the current day $T_{\min}$, daily total rainfall for the current day R_t, daily total snowfall for the current day S_t, daily snow on the ground depth for the current day SG_t, daily snow on the ground depth for the previous day SG_{t-1}, the current daily stream flow F_t, and the previous daily stream flow F_{t-1}. Twenty models were developed for each lead time. Only the best model for each lead time is provided in Tables X to XIII. All of the ANN models were first trained using the data in the training set (1951 to 1979) to obtain the optimized set of connection strengths, and then tested using the testing data set (1980 to 1983), and compared using the three statistical measures of goodness of fit.

The best model for 1 day lead time, ANN (1)-2, is a function of daily stream flow for the previous day, daily snow depth on the ground for the current day, daily snow depth on the ground for the previous day, daily total rainfall for the current day, daily total snowfall for the current day, and maximum temperature for the current day. This model had a 6-6-1 architecture and an optimized learning coefficient of 0·05.

The best model for 3 days lead time, ANN (3)-5, is a function of daily stream flow for the current day, daily stream flow for the previous day, daily snow depth on the ground for the current day, daily snow depth on the ground for the previous day, daily total rainfall for the current day, daily total snowfall for the current day, and maximum temperature for the current day. This model had a 7-6-1 architecture and an optimized learning coefficient of 0·04.

The best model for 7 days lead time, ANN (7)-3, is a function of daily stream flow for the current day, daily stream flow for the previous day, daily snow depth on the ground for the current day, daily snow depth on the ground for the previous day, daily total rainfall for the current day, daily total snowfall for the current day, and maximum temperature for the current day. This model had a 7-6-1 architecture and an optimized learning coefficient of 0·04.

Proposed stand-alone wavelet flood forecasting method

The proposed stand-alone flood forecasting method based on wavelet and cross–wavelet constituent components is composed of the following steps:

1. Data editing
In order to reduce the number of variables in wavelet analysis, the variable 'precipitation' (P) was calculated using:

$$P = \mathrm{Rain}(t) + \mathrm{Snow}(t) + [\mathrm{SnowonGround}(t-1) - \mathrm{SnowonGround}(t)] \quad (12)$$

with P in mm.

2. Overview wavelet analysis
Overview wavelet analysis was conducted using the CWTA.F software in UNIX. In the overview wavelet analysis, the scales used ranged from 2 to 21 180 days and the translation (or shifting interval) used was 10·5 days. Overview wavelet analysis was done on the flow F, precipitation P, minimum temperature TI, and maximum temperature TA variables. The waveband subtitles (i.e. the designation for the individual wavebands found to be the most significant in the overview wavelet analysis, and subsequently confirmed through histograms and spectral analysis) for the results of the wavelet analysis are shown in Table I.

Table I. Waveband subtitles for wavelet analysis

Waveband (days)	9–13	22–28	44–52	90–130	330–400
Waveband subtitle	11	25	48	100	365

Table II. Waveband subtitle for cross–wavelet analysis

Waveband (days)	330–400
Waveband subtitle	365*x*

3. Cross-wavelet analysis
Cross-wavelet analysis was performed with a software program entitled XCWT.F (Prokoph, 2006), which was very recently created as a companion software program for the CWTA.F software. Cross-wavelet analysis (XWA) was used to check for potential coherency between the cycles in the flow and meteorological data, to obtain actual phase differences between flow and meteorological cycles, and to construct cross-wavelet constituent signals. The waveband subtitles for the cross-wavelet analysis are shown in Table II.

4. Calculation of histograms
Histograms were created from the wavelength columns of the wavelet analysis results from the decomposition of flow, precipitation, and maximum and minimum temperature, in order to determine the frequency peaks, and to determine whether the same signals occur in the meteorological data as in the flow data so that the former can be used to effectively forecast the latter. In this manner, it was determined which wavelengths (periods) occurred most frequently and should therefore possibly be used in the construction of the forecasting models. The choice of signals was confirmed via power spectra.

5. Spectral analysis
Spectral analysis was used to confirm the results of the overview wavelet analysis (major wavebands) and histograms (major wavebands) in terms of the choice of major wavebands (for example 330 to 400 days) to be used in the reconstruction and forecasting models.

6. Narrowband wavelet analysis
Narrowband wavelet decomposition analysis was used to decompose the selected wavebands. The software program detects and extracts the strongest wavelength within a specific waveband at time t, along with the corresponding phase at time t, and the amplitude at time t.

This step was done on the selected wavebands on all variables (i.e. F, P, TI, and TA). Various scales were used for narrowband wavelet analysis. Scales of 2 to 200 days were used for TI and TA, while for the rest of the variables the wavebands in the models/components for extraction were used for all variables (e.g. 330–400 days for $\sim$365 day cycles, 90–130 days for $\sim$100 day cycles, 44–52 days for $\sim$48 day cycles, 22–28 days for $\sim$25 day cycles, and 9–13 days for $\sim$11 day cycles). The translation used in the narrowband wavelet analysis was 1 day.

7. Calculation of edge effects

The 'Morlet wavelet edge effect' is characterized by decreased wavelet coefficients at the beginning and end of the data sets (in the case of this research at the beginning of 1951 and end of 1979) due to the window width of the Morlet wavelet used. Due to the fact that the longest wavelength used (∼365 days) is only about 3% of the entire record (∼12 053 days) only the very beginning and end of the data sets are influenced by edge effects. The shorter components (such as 9–13, 22–28, 44–52, and 90–130 days) are even less affected. As such, although the edge effect is large for long wavelengths (defined as over one half the entire data record) in other applications, it is negligible in this application since all cycles are comparably small (much smaller than half the entire data record length). However, an edge effect correction factor was still calculated and applied in the reconstruction of the constituent signals for the sake of completeness since minor edge effects do occur in the first and last years of training (ie 1951 and 1979). The edge effect correction for the Morlet wavelet edge effect involved dividing the continuous wavelet transform outputs of amplitude of a waveband *x*/amplitude of a cosine wave with amplitude 1. This is shown by:

$$Y_{n',s} = 1/W_{cosn',s} \tag{13}$$

where n' is time, s is the waveband (e.g. 40–45 days), $Y_{n',s}$ is the Morlet wavelet edge effect correction, and $W_{cosn',s}$ is the amplitude of a cosine wave with amplitude 1.

8. Calculation of calibration constants

A calibration constant was developed in this study which calibrates (or links) meteorological components to flow components. The calibration constant is the ratio in amplitude between each specific wavelength, and it permits forecasting of flow data by meteorological data by calibrating the meteorological components to the flow components of the same wavelength (e.g. temperature cycle to river flow cycle).

Calculation of calibration constants was done for the selected wavebands for *P*, *TI*, and *TA*. Each single day (i.e. 10 593 days) of training data was used to calculate the calibration constants. The calibration constant $Z_{n',s}$ for each meteorological variable for each component was calculated by dividing the amplitude of the meteorological cycle from the corresponding amplitude of the flow cycle, and is shown by:

$$Z_{n',s} = [W_{n',s(\text{flowdata})}]/[W_{n',s(\text{meteorologicaldata})}] \tag{14}$$

9. Reconstruction of constitutive series

From the above steps, the following was derived: (1) amplitude (i.e. wavelet coefficient) for each Julian day, for each constituent component, for each variable (flow and meteorological); (2) wavelength for each Julian day, for each constitutive component, for each variable (flow and meteorological); (3) phase difference and phase for each constitutive component of each variable for each Julian day; (4) edge effect correction for each variable for each Julian day; and (5) calibration constant for each constitutive component of each meteorological variable. The average values of the above are shown in Tables III to VIII.

All of the above information was used to reconstruct two types of constitutive components: wavelet constitutive components and cross wavelet constitutive components.

The wavelet constitutive components were reconstructed through the inverse Fourier transform multiplied by a calibration constant and an edge effect correction, along with a phase difference. For reconstruction, the

Table III. Average amplitude for each wavelet component

Waveband	Average amplitude ($m^3\ s^{-1}$)					
	9–13	22–28	44–52	90–130	330–400	330–400*x*
Component	11	25	48	100	365	365*x*
Flow (*F*)	1·0215	1·5194	2·0955	2·8105	3·7699	3·3948
Tmin (*TI*)	1·8259	1·7211	1·6741	1·3451	8·5925	7·9344
Tmax (*TA*)	2·0387	1·9837	1·8228	1·4322	11·618	10·767
Precipitation (*P*)	1·3954	0·9504	0·8066	0·6391	0·6631	0·5951

Table IV. Average wavelength for each wavelet component

Waveband	Average Wavelength (days)					
	9–13	22–28	44–52	90–130	330–400	330–400*x*
Component	11	25	48	100	365	365*x*
Flow (*F*)	11·57	24·239	49·979	111·04	362·9	365·25
Tmin (*TI*)	10·888	23·887	46·952	108·25	364·88	365·25
Tmax (*TA*)	10·994	23·968	47·26	106·08	364·67	365·25
Precipitation (*P*)	10·792	23·79	45·898	101·85	360·74	365·25

DOI: 10.1002/hyp

Table V. Phase difference for flow $F(t)$ at $t = 1$: 1 January 1951

Waveband	Phase difference for $t = 1$					
	9–13	22–28	44–52	90–130	330–400	330–400x
Component	11	25	48	100	365	365x
Tmin (*TI*)	0	+0·3	−0·3	+0·7	−2·2	+2·2
Tmax (*TA*)	0	+0·3	−1·7	−2·5	−2·4	+2·4
Precipitation (*P*)	+0·8	+0·8	+0·8	+0·1	−2·45	+2·45

Table VI. Phase for each wavelet component at $t = 1$: 1 January 1951

Waveband	Phase for $t = 1$					
	9–13	22–28	44–52	90–130	330–400	330–400x
Component	11	25	48	100	365	365x
Flow (*F*)	−0·819	1·3252	2·8683	−2·211	1·305	1·0939
Tmin (*T*I)	2·6342	−0·93	−1·22	−1·601	−2·84	−2·758
Tmax (*TA*)	−2·778	−0·307	−1·547	−1·625	−2·914	−2·833
Precipitation (*P*)	1·6577	−1·687	1·4621	−2·08	−2·392	−2·904

Table VII. Average edge effect correction for each waveband

	Edge effect correction for long meteorological cycles
365 days	1·087
100 days	1·0707
48 days	1·0675
25 days	1·0658
11 days	1·0651

Table VIII. Average calibration constants

Unit (days)	Average attenuation/Calibration constant		
	Tmin	Tmax	Precipitation
	m^3 s^{-1}/C	m^3 s^{-1}/C	m^3 s^{-1}/mm
365days	0·427854	0·315280	5·704420
100days	2·089395	1·962316	4·397705
48 day	1·251725	1·149576	2·597769
25 days	0·882832	0·765953	1·598703
11 days	0·559468	0·501059	0·732061

wavelet coefficients (ie amplitude) were assumed to be equal to the Fourier amplitudes, and the Morlet wavelet scales were assumed to be equal to the Fourier period. An assumption that was made was that there is a linear relationship between changes in amplitude of meteorological signals (e.g. temperature, precipitation cycles) and streamflow cycles, with particular calibration constants and differences in phase. Including the calibration constant $Z_{n',s}$, the edge effect correction $Y_{n',s}$, the phase difference $\Delta\phi_{n',s}$ between a meteorological component and its corresponding flow component, and noting that s defines the individual waveband (e.g. 40–45 days), while $s_{n'}$ defines the strongest wavelength inside the waveband s at location (or time) n', each wavelet constitutive component was reconstructed for each Julian day by:

$$x_{n',s} = Z_{n',s}Y_{n',s}W_{n',s}\left(\cos 2\pi\frac{n'}{s_{n'}} + \phi_{n',s} + \Delta\phi_{n',s}\right) \quad (15)$$

The parameters in the above equations vary through the year for each day, and as such explicitly take into account the daily non-stationarities in the data. In other words, there are separate constitutive series (and therefore forecasting models) for each specific day from 1 January to 30 June (the testing period the models were developed for). This is how the models should be used in an operational context. Only average values of the parameters are presented in the tables for the sake of succinctness.

The cross-wavelet components (designated by x in the series such as $TI\,365x$) were calculated from the cross–wavelet analysis of each variable with a 365-day cosine wave to avoid phase-averaging between $-\pi$ and $+\pi$, which sometimes resulted in short-time jumps in the reconstructed constituent component. The cross-wavelet transform of each variable (for example F) and a continuous cosine wave with the mean wavelength of the band (~365 days) and fixed amplitude of 1, was performed. From (4) and (15), the cross-wavelet constituent components can be described as:

$$xy_{n',s} = Y_{n,'s,x,y}W_{n',s,x,y}(\cos^2 2\pi n'/s_{n'} + \Delta\phi_{n',s,x,y}) \quad (16)$$

By using a cosine wave with amplitude = 1 as variable y and $\phi_{n',s,y}$ continuously changing in time, the only variables are $W_{n',s,x}$ and $\phi_{n',s,x}$ and as such, $W_{n',s,x,y}$ and $\Delta\phi_{n',s,x,y}$ are solely related to the non–cosine variable. Another advantage is that $\Delta\phi$ may vary little, because it is related to the continuous phase changes in the cosine wave. As such, unwanted numerical artifacts in the phase transition from π to $-\pi$ may be replaced by a fixed $\Delta\phi$

Table IX. Average values for cross-wavelet constituent components

Cosine cycle vs 365 days	*F*	*TA*	*TI*	*P*
Mean wavelength	363·5718	364·1383	364·0621	364·3678
Phase shift	1·11809	−2·86943	−2·76666	−1·9322
Cross amplitude	4·039346	12·62865	9·301946	0·693421

and a variable time n'. It was found that this replacement worked well for the annual (i.e. 365 day) components in the Skrwa Prawa River case but not for components of shorter wavelength with more variable phase values. The average values for the cross wavelet constituent components are shown in Table IX.

10. Calculation of averaged reconstructed constituent components

The reconstructed daily constituent components (i.e. Equations (15) and (16)) were averaged for the same Julian day year-to-year for each day of the training period for the 1 January to 30 June period, and not the phase, amplitude, and wavelengths for each model. These averaged daily reconstructed components were then used in the construction of the forecasting models. This averaging assumed that there was no significant trend in the amplitudes, and that a relatively stable phase shift (i.e. phase difference) existed between F and the meteorological signals for the same Julian day year-to-year. No significant trends in the amplitudes was found, and the cross-wavelet scalogram and phase difference spectrum (shown in Figure 2) indicated a relatively stable phase shift between F and the meteorological signals.

11. Construction of forecasting models

The best constructed wavelet forecasting models for 1, 3, and 7 days lead time are shown in Tables X, XI, and XII, respectively. An assumption that was made in the construction of the wavelet based models was that, in an operational context, one would have access to data for the flow $F(t)$ up to and including the $F(t)$ day. The wavelet-based forecasting models for the Skrwa Prawa River were constructed from:

(a) the flow data of the previous day (or 3 days ago or 7 days ago) plus
(b) the difference between the current day cyclical output from a 365 day cross-wavelet constitutive series-y and the previous day cyclical output from the same 365 day cross-wavelet constitutive series-y (or 3 days ago or 7 days ago) and, in some cases, plus
(c) the difference between the current day cyclical output from a regular constitutive series-y and the previous day cyclical output from the same constitutive series-y (or 3 days ago or 7 days ago), or more cycles of this type.

As shown in Tables I andII, the waveband subtitles 365x, 365, 100, 48, 25, and 11 for F, P, TA, and TI used in the forecasting models are simply 'designations' since the actual wavelength values (in addition to all other values) vary on a day to day basis. On a day–to–day basis, the ~365 day 'wavelengths' can vary from 330 to 400 days, the ~100 day 'wavelengths' from 90 to 130 days, the ~48 day 'wavelengths' from 44 to 52 days, the ~25 day 'wavelengths' from 22 to 28 days, and the ~11 day 'wavelengths' from 9 to 13 days. As an example, $TA100$ is the designation within which can be found, for a specific day, the most significant wavelength within the 90 to 130 day waveband (designated as 100) for the maximum temperature (designated as TA) for that specific day. As mentioned earlier, the most significant wavelength for each day within each of the five wavebands for each of the variables F, P, TA, and TI was found through wavelet analysis and confirmed through the use of histograms and spectral analysis.

The high number of components allows for a very large number of possible combinations for models. In order to obtain the best possible overall wavelet model, stepwise correlation was used for optimization. The best wavelet model was constructed by assessing the correlation (R^2) of each component with the training $F(t)$, and taking the best correlating components as the basis and adding the other components successively to the model depending on whether the forecast improved or not.

The best overall wavelet model for 1 day lead time, WT (1)—M23, is shown in Table X and can be written as

$$F(t-1) + [P365x(t) - P365x(t-1)] + [TA100(t) - TA100(t-1)] + [P48(t) - P48(t-1)] + [P25(t) - P25(t-1)] + [TI11(t) - TI11(t-1)]$$

This model was developed based on the flow from the day before, the difference between the current day output from the 365 day cross-wavelet constitutive cycle of the precipitation and the previous day output of the same cross-wavelet constitutive cycle, and the difference between the current day output from each constitutive cycle of a variety of components, and the previous day output from each constitutive cycle of a variety of components.

The best overall wavelet model for 3 days lead time, WT (3)—M23, is shown in Table XI and can be written as

$$F(t-3) + [P365x(t) - P365x(t-3)] + [TA100(t) - TA100(t-3)] + [P48(t) - P48(t-3)] + [P25(t) - P25(t-3)] + [TI11(t) - TI11(t-3)]$$

DOI: 10.1002/hyp

Table X. Components for best 1 day lead time WT model and ANN model

Model	Constituent components for best 1 day lead time forecasting model
WT (1)–M23	$F(t-1)+P365x(t)-P365x(t-1)+TA100(t)-TA100(t-1)+P48(t)-P48(t-1)+P25(t)-P25(t-1)+TI11(t)-TI11(t-1)$
ANN (1)–2	Tmax, Rt, St, SGt, SGt-1, Ft-1 (learning coefficient 0·05)

Table XI. Components for best 3 days lead time WT model and ANN model

Model	Constituent components for best 3 days lead time forecasting model
WT (3)–M23	$F(t-3)+P365x(t)-P365x(t-3)+TA100(t)-TA100(t-3)+P48(t)-P48(t-3)+P25(t)-P25(t-3)+TI11(t)-TI11(t-3)$
ANN (3)–5	Tmax, Rt, St, SGt, SGt-1, Ft, Ft-1 (learning coefficient 0·04)

Table XII. Components for best 7 days lead time WT model and ANN model

Model	Constituent components for best 7 days lead time forecasting model
WT (7)–M23	$F(t-7)+P365x(t)-P365x(t-7)+TA100(t)-TA100(t-7)+P48(t)-P48(t-7)+P25(t)-P25(t-7)+TI11(t)-TI11(t-7)$
ANN (7)–3	Tmax, Rt, St, SGt, SGt-1, Ft, Ft-1 (learning coefficient 0·04)

The best overall wavelet model for 7 days lead time, WT (7)—M23, is shown in Table XII and can be written as

$$F(t-7)+[P365x(t)-P365x(t-7)]$$
$$+[TA100(t)-TA100(t-7)]+[P48(t)-P48(t-7)]$$
$$+[P25(t)-P25(t-7)]+[TI11(t)-TI11(t-7)]$$

In an operational context, the above models would be used with the component parameter values from the specific day to be forecasted and component parameter values from the current day needed to forecast the flow for that specific day. The flow value for the current day would also be used. For example, in the case of 7 days lead time forecasting, model WT (7)—M23 would be used as follows in an operational context

$$F(t+7)=F(t)+[P365x(t+7)-P365x(t)]$$
$$+[TA100(t+7)-TA100(t)]+[P48(t+7)-P48(t)]$$
$$+[P25(t+7)-P25(t)]+[TI11(t+7)-TI11(t)]$$

where the only 'external' value needed is the $F(t)$ value, which would be obtained from the flow station for that current day, and with all other values having already been calculated for that specific day in the development of the forecasting models.

12. Testing of constructed forecasting models

The wavelet (WT) models were tested on data from 1980 to 1983 by comparing the original F(t) or observed flow with the forecasted output of the models. Models were compared using the coefficient of determination (R^2), the efficiency index (EI), and the root mean square error (RMSE). A simple perseverance model for flow was also tested for comparative purposes.

RESULTS

Overview wavelet analysis

All wavebands were found using the continuous wavelet transform and confirmed with the use of histograms and power spectra. In total, five major wavebands were identified: a dominant and stationary 365 day cycle, and weaker, non–stationary cycles of approximately 11, 25, 48, and 100 day cycles. These are shown in Table I. No significant multiyear signals were found.

Overview wavelet scalograms and phase spectrum figures

From the overview wavelet scalogram of the flow data in Figure 1, one can visually see the stationarity of the 365 day cycle (a horizontal line indicates stationarity). However, it is more difficult to visually see the <365 day wavebands. The reason for this is that the colour scale is linear between 0 and the maximum, and because the maximum waveband ($\sim$365 days) is strong, it suppressed the other wavelengths.

Cross–wavelet analysis

Cross–wavelet analysis was first used to assess the correlation in phase (i.e. whether there is a relatively stable phase shift) between the meteorological and flow data series for the same Julian day year-to-year since otherwise, averaging in the forecasting/modeling stage would cause problems with the phase information. It was found that the correlation in phase was relatively stable. This indicated that the meteorological parameters could be used to forecast flow. As such, cross-wavelet analysis was used to determine the specific phase difference values between F and meteorological variables. The phase differences at $t=1$ can be found in Table V.

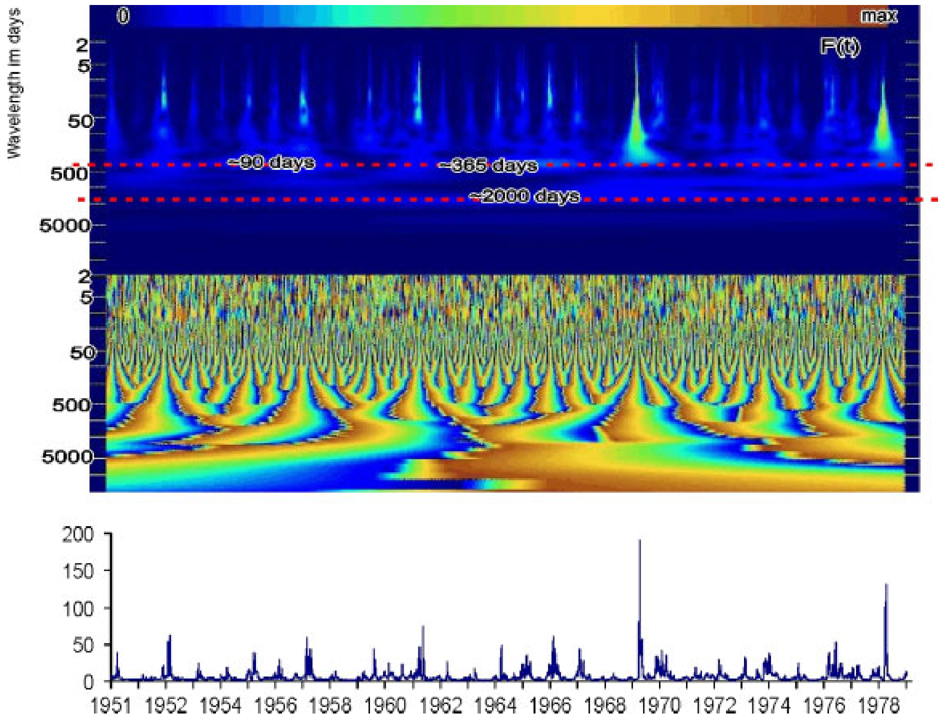

Figure 1. Overview of wavelet analysis of Skrwa-Prawa traning flow data

In order to overcome a $-\pi$ to $+\pi$ averaging problem that occurred occasionally with the Skrwa Prawa data, cross-wavelet constituent components were developed. Based on exploratory analysis, it was found that developing cross-wavelet constituent components worked well for the annual (i.e. 365 day) components, but not for the shorter components that changed to a more significant degree with time. Thus, only cross-wavelet constituent 365 day components of all variables were used in the development of the forecasting models. Table II shows the waveband subtitle for the cross-wavelet constituent component. Table IX shows the average cross–wavelet constituent component analysis results for the 365 day cycles of each variable in terms of mean wavelength, phase shift and edge effect corrected cross-amplitude.

Cross-wavelet scalogram and phase difference spectrum figures

From the cross-wavelet scalograms (the top figures) of the logarithmically spaced flow data with the precipitation, minimum temperature, and maximum temperature data shown in Figure 2, one can visually see the dominance of the relatively stationary 365 day cycle (the horizontal band). A horizontal line indicates stationarity.

An observation that can be made from the cross-wavelet analysis figures is that the *TI* and *TA* 365 day cycles stand out much stronger than the *P*365 cycle, yet the *P*365 cycle turned out to be more useful than the *TI* and *TA* 365 day cycles in the forecasting models. This demonstrates that it is not the strength (amplitude/magnitude) by itself that is important, but the consistency of the link between $F(t)$ and the variable which is decisive.

Histograms

The histograms of the frequency of signal occurrences from the wavelet analysis of the flow data and the meteorological data indicated that strong peaks occur at approximately 330–400 days, 90–130 days, 44–52 days, 22–28 days, and 9–13 days for the flow and meteorological data. The histogram for flow data is shown in Figure 3.

Power spectra

The results of the power spectra confirmed the results of the overview wavelet analysis and histograms in terms of the choice of the five major wavebands (i.e. approximately 11, 25, 48, 100, and 365 day cycles). The power spectra for flow data is shown in Figure 4.

Results of best wavelet and ANN model for 1 day lead time forecasting

The calculated performance statistics for the best wavelet and ANN model are shown in Table XIII for the training and testing stages. The performance statistics for the perseverance 'model' PM (1) is also shown in Table XIII. It was found that the best wavelet model for 1 day lead time forecasting is WT (1)—M23. Model WT (1)—M23 had the lowest testing RMSE, and the highest testing R^2 and EI values:

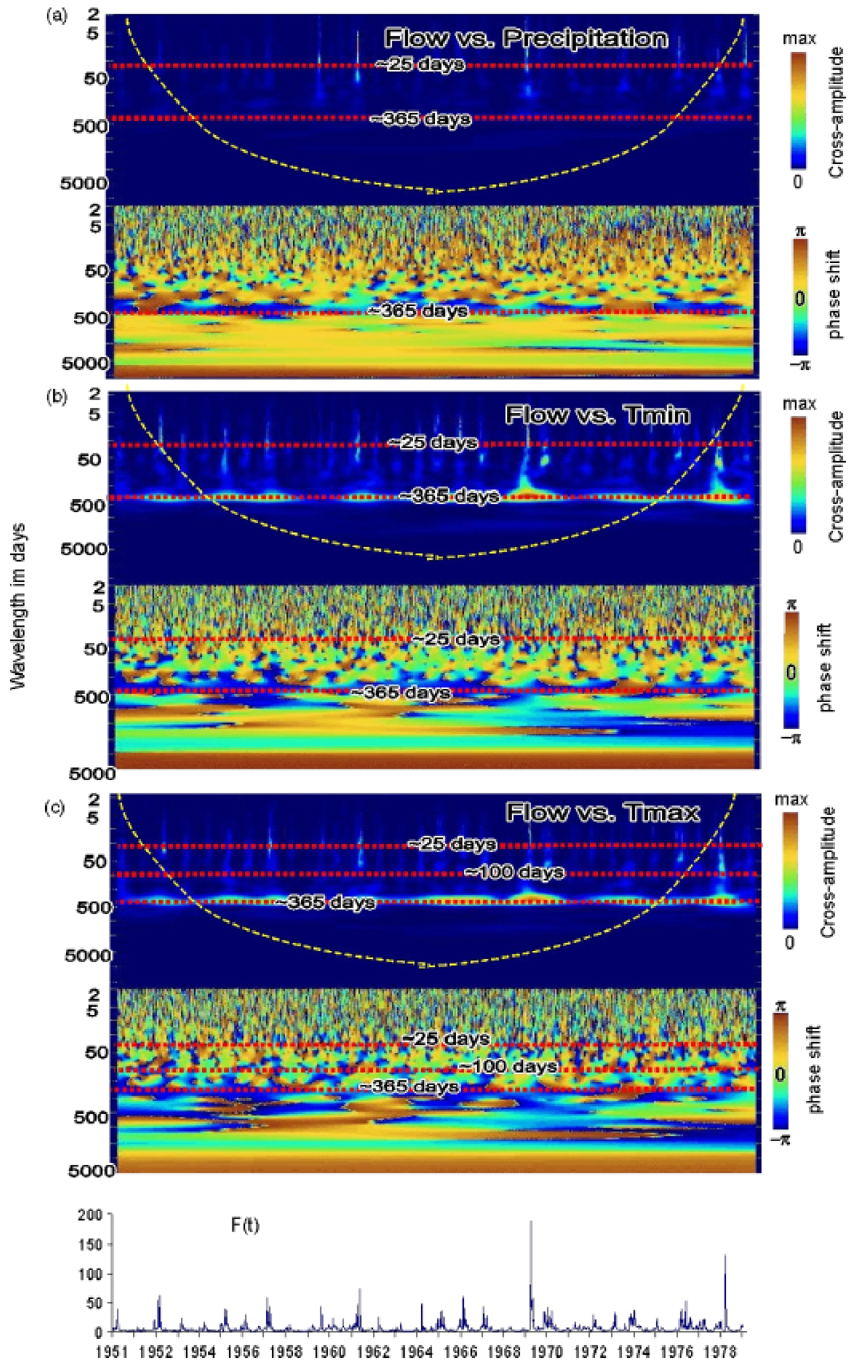

Figure 2. Cross-wavelet analysis of Skrwa-Prawa River training data

Table XIII. Performance statistics for best WT model, perseverance model, and ANN model for 1 day lead time

Wavelet Model	RMSE Training	RMSE Testing	R^2 Training	R^2 Testing	EI Testing
WT(1)–M23	2·2653	2·4325	0·9453	0·9405	0·9366
PM (1)		3·0894		0·9151	0·9132
ANN(1)–2	2·4583	2·6271	0·9235	0·9205	0·9211

- The root mean square error was 2·2653 and 2·4325 for training and testing respectively.
- The coefficient of determination was 0·9453 and 0·9405 for training and testing respectively.
- The efficiency index was 0·9366 for testing.

This model can be written as

$$\begin{aligned} \text{WT (1)} - \text{M23} &= F(t-1) + [P365x(t) \\ &\quad - P365x(t-1)] + [TA100(t) - TA100(t-1)] \\ &\quad + [P48(t) - P48(t-1)] + [P25(t) - P25(t-1)] \\ &\quad + [TI11(t) - TI11(t-1)] \end{aligned}$$

In terms of the testing RMSE, WT (1)—M23 was 27% more accurate than the 1 day perseverance model PM (1), and 0·8% more accurate than the best 1 day ANN model ANN (1)-2. In terms of the testing R^2, WT (1)—M23

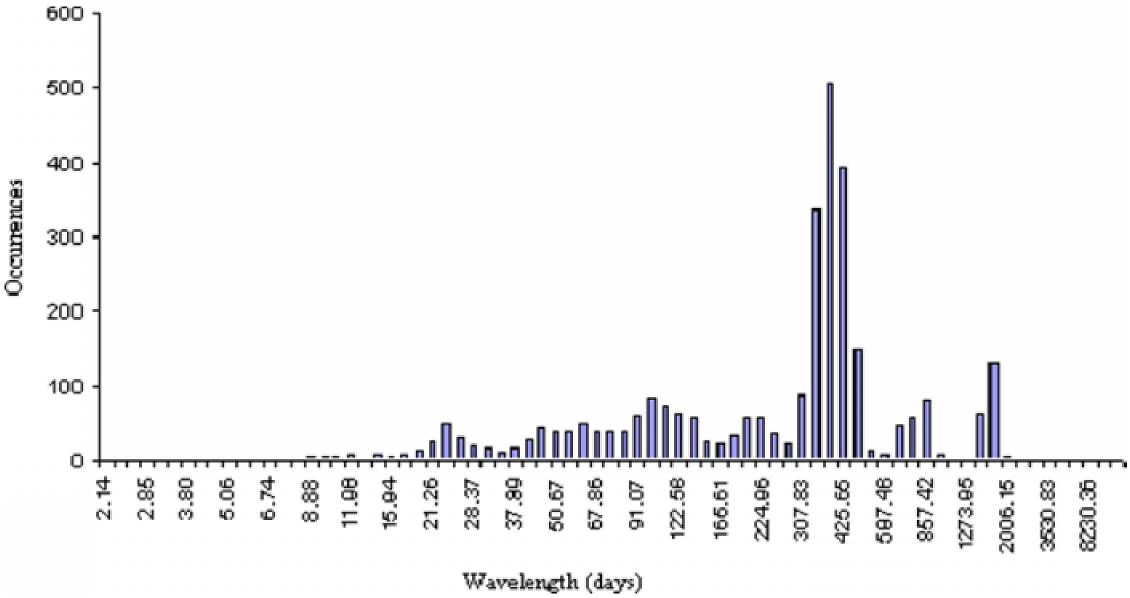

Figure 3. Histogram of signal occurrences in Skrwa-Prawa River training flow data

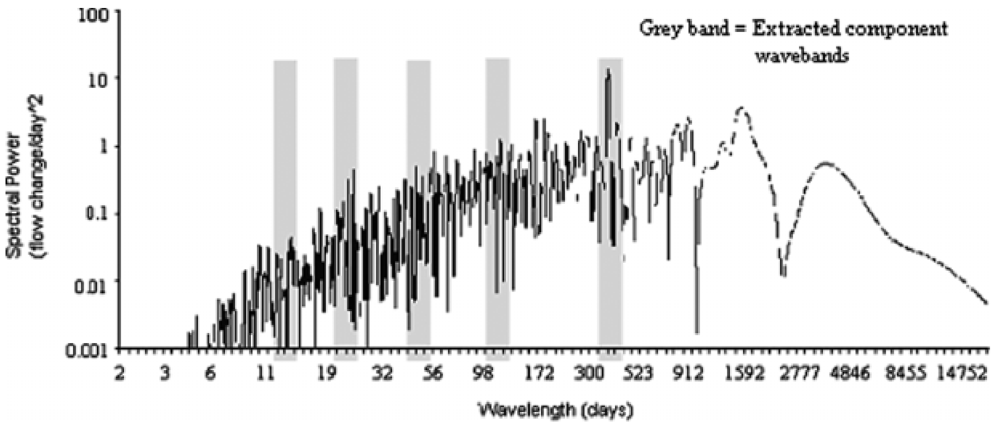

Figure 4. Power spectra of Skrwa Prawa River flow data

was 2·7% more accurate than the 1 day perseverance model, and 2·1% more accurate than ANN (1)-2. And in terms of the testing EI, WT (1)—M23 was 2·5% more accurate than the 1 day perseverance model, and 1·7% more accurate than ANN (1)-2.

Figure 5 compares the observed and forecasted flow from model WT (1)—M23. It can be seen that low, medium, and high flows were very accurately forecasted.

Results of best wavelet and ANN model for 3 days lead time forecasting

The calculated performance statistics for the best wavelet and ANN model are shown in Table XIV for the training and testing stages. The best wavelet model for 3 days lead time forecasting was WT (3)—M23. Model WT (3)—M23 had the lowest testing RMSE, the highest testing EI value, and the highest testing R^2 value:

- The root mean square error was 4·9563 and 5·6348 for training and testing respectively.
- The coefficient of determination was 0·7654 and 0·6598 for training and testing respectively.
- The efficiency index was 0·6218 for testing.

This model can be written as

$$\begin{aligned} WT\ (3) - M23 &= F(t-3) + [P365x(t) \\ &\quad - P365x(t-3)] + [TA100(t) - TA100(t-3)] \\ &\quad + [P48(t) - P48(t-3)] + [P25(t) - P25(t-3)] \\ &\quad + [TI11(t) - TI11(t-3)] \end{aligned}$$

In terms of the testing RMSE, WT (3)—M23 was 29% more accurate than the 3 day perseverance model PM (3),

Table XIV. Performance statistics for best WT model, perseverance model, and ANN model for 3 days lead time

Wavelet Model	RMSE Training	RMSE Testing	R^2 Training	R^2 Testing	EI Testing
WT(3)–M23	4·9563	5·6348	0·7654	0·6598	0·6218
PM (3)		7·2689		0·5791	−0·5211
ANN(3)–5	5·2818	5·9618	0·7423	0·6428	0·6088

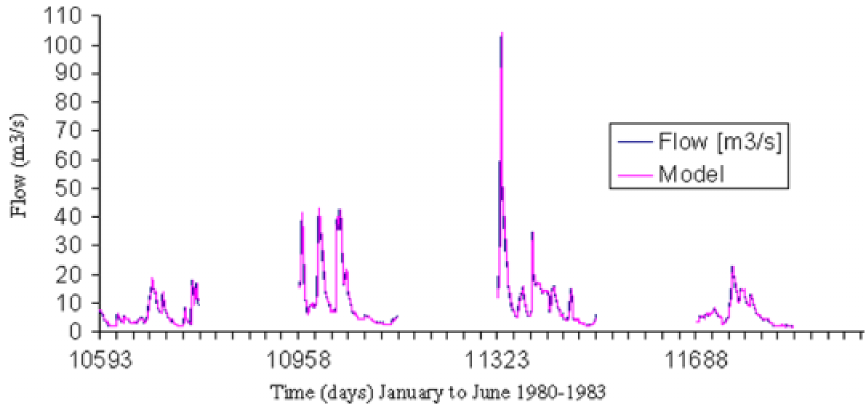

Figure 5. Best WT model for 1 day lead time (WT(1)–M23)

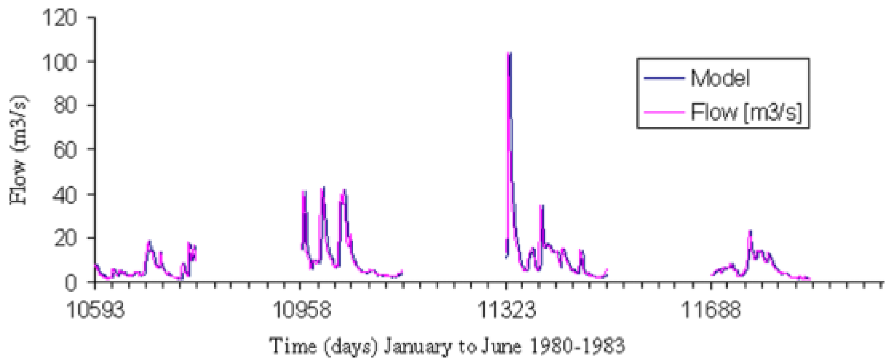

Figure 6. Best WT model for 3 days lead time(WT(3)–M23)

and 0·58% more accurate than the best 3 day ANN model ANN (3)-5. In terms of the testing R^2, WT (3)—M23 was 12·2% more accurate than the 3 day perseverance model, and 2·51% more accurate than ANN (3)-5. And in terms of the testing EI, WT (3)—M23 was 16·2% more accurate than the 3 day perseverance model, and 2·1% more accurate than ANN (3)-5.

Figure 6 compares the observed and forecasted flow using model WT (3)—M23. The forecasted stream flow does not match the observed flow as well as in case of the 1 day lead time forecast. For the WT (3)—M23 model, a slight shift to the right in the forecasted flow can be observed.

Results of best wavelet model for 7 days lead time forecasting

The calculated performance statistics for the best wavelet and ANN model are shown in Table XV for the training and testing stages. The best wavelet model for 7 days lead time forecasting was WT (7)—M23. Model WT (7)—M23 had the lowest testing RMSE, the highest testing EI, and the highest testing R^2:

- The root mean square error was 6·6869 and 8·7671 for training and testing respectively.
- The coefficient of determination was 0·5721 and 0·2552 for training and testing respectively.
- The efficiency index was −0·0398 for testing.

Table XV. Performance statistics for best WT model, perseverance model, and ANN model for 7 days lead time

Wavelet Model	RMSE Training	RMSE Testing	R^2 Training	R^2 Testing	EI Testing
WT(7)–M23	6·6869	8·7671	0·5729	0·2552	−0·0398
PM (7)		11·5550		0·1608	−0·2036
ANN(7)–3	5·1179	7·4297	0·6913	0·3190	−0·0283

This model can be written as

$$\begin{aligned} \text{WT (7)} - \text{M23} = {} & F(t-7) + [P365x(t) \\ & - P365x(t-7)] + [TA100(t) - TA100(t-7)] \\ & + [P48(t) - P48(t-7)] + [P25(t) - P25(t-7)] \\ & + [TI11(t) - TI11(t-7)] \end{aligned}$$

In terms of the testing RMSE, WT (7)—M23 was 31·8% more accurate than the 7 day perseverance model PM (7), but 18% less accurate than the best 7 day ANN model ANN (7)-3. In terms of the testing R^2, WT (7)—M23 was 37% more accurate than the 7 day perseverance model, but 33·2% less accurate than ANN (7) 3. And in terms of the testing EI, WT (7)—M23 was 81% more accurate than the 7 day perseverance model, but 41% less accurate than ANN (7)-3.

Figure 7 compares the observed and forecasted flow using model WT (7)—M23. It can be seen that in the case of a 7 day lead time forecast, the forecasted stream

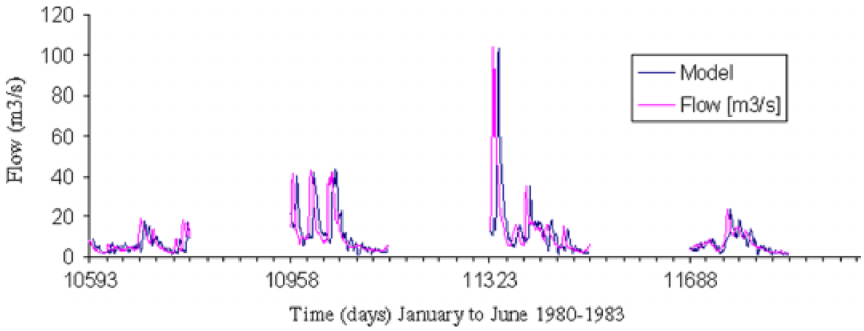

Figure 7. Best WT model for 7 days lead time (WT(7)–M23)

flow does not match the observed flow very well. For the WT (7)—M23 model, a significant shift to the right in the forecasted flow can be observed.

DISCUSSION AND CONCLUSION

Best wavelet model

The best wavelet model for 1, 3, and 7 days lead–time forecasting was 'model M23' which can be described, for example in the case of 3 days lead time forecasting, by

$$F(t-3)+[P365x(t)-P365x(t-3)]+[TA100(t)-TA100(t-3)]+[P48(t)-P48(t-3)]+[P25(t)-P25(t-3)]+[TI11(t)-TI11(t-3)]$$

This is a 'mixed' variable and signal model. It can be seen that in the case of the Skrwa Prawa River, the changes in cyclical outputs of the variables P, TI, and TA with varying wavelengths (i.e. 365, 100, 48, 25, and 11 days) provided the most accurate forecasting model. More specifically, it was found that the $\sim$365 day precipitation cycles ($P365x$), the $\sim$100 day maximum temperature cycles ($TA100$), the $\sim$48 day precipitation cycles ($P48$), the $\sim$25 day precipitation cycles ($P25$), and the $\sim$11 day minimum temperature cycles ($TI11$), provided the most accurate forecasting models for 1, 3, and 7 days flood forecasting. Aside from this, any further physical insight regarding the composition of the wavelet models is difficult to provide.

Low accuracy of 7 days lead–time forecasting with wavelet model

The wavelet model for 7 days lead time forecasting was not accurate, with the ANN model providing more accurate results. It was difficult to find any 'technical' reason as to why the 7 days lead time wavelet forecasting model was not very accurate. Most likely, the averaging that is necessary for the wavelet forecasting models affects the longer forecasts to a greater degree.

Artificially splitting the training data

To obtain the best possible wavelet forecasting models, one must carefully consider the following two issues: (a) split the data artificially so that the constituent components only deal with the period of interest for forecasting, but have potentially significant edge effect problems and possibly phase problems; or (b) not split the data artificially so that the constituent components deal with the entire year and as such not have potentially significant edge effect or phase problems, but have unwanted remains of influences of cycles from the period of the year not being forecasted.

It is very difficult to decide *a priori* (before analysis/modeling starts) if the artificial splitting of the data would have a large or small effect on particular wavebands and variables. To determine whether it is advisable to artificially split the data, it would be necessary to analyse the cut data in great detail. For example, if the causes of floods are completely different at certain points of the year (which is often the case), artificially splitting the data for those specific periods should be considered. Wavelet-based forecasting models could then be developed specifically for those periods.

Based on the results of this study, the $\sim$365 day cycle (or whatever 'annual' cycle results from the split data) would improve if the data was split, but the other cycles would deteriorate. For the Skrwa Prawa River, hydrologists have observed that it is difficult to decide when the 'winter-influence' on floods begin, since it can be seen from the data that some 'winter-floods' occur as early as the end of December. It is difficult to ascertain whether it would be advisable to artificially cut the data in the future for other applications (including the Skrwa Prawa River) to obtain more accurate forecasting models.

Based on the results of this study, the author recommends the use of *unsplit* data for training in any future applications with other watersheds, even if there will be unwanted remains of influences of cycles from the period of the year not used for forecasting (for example the July–December period in the Skrwa Prawa River case). On a related note, the author recommends the use of approximately ten years of daily data to develop wavelet and cross–wavelet transform models such as those proposed in this research.

Cross-wavelet constituent components

The cross-wavelet constituent components developed in this study were calculated from the cross-wavelet analysis of each variable with a 365-day cosine wave to avoid phase averaging between the $-\pi$ and $+\pi$ transition, which occasionally results in short-time jumps in the reconstructed components. If it is necessary to develop cross-wavelet constituent signals for the flood forecasting models due to problems with averaging of the transition between $-\pi$ and $+\pi$, then this should be done since it provides more accurate results. The reason why the 365 day cross wavelet constituent components (i.e. 365*x*) were superior to the 'regular' 365 day constituent components is that the 365*x* components did not have the occasional problematic phase error that appeared in the transition between $-\pi$ and $+\pi$ in the ϕ_{lix} alone.

Summary

There are a number of issues with respect to the use of wavelet and cross-wavelet analysis for flood forecasting within the area of hydrology that were explored in this study that, to the best knowledge of the author, have not been explored in any great detail in the literature. The main conclusions of this research are:

1. The use of wavelet analysis in the development of a stand-alone wavelet-based short-term river flood forecasting method was shown to be useful for 1 and 3 day lead time forecasting, assuming that there are no *significant* trends in the amplitude for the same Julian day year-to-year. The use of wavelet derived daily constituent components for flood forecasting that take into account the day-to-day non-stationarity of flow and meteorological time series allowed for the exploitation of one of the strengths of wavelet analysis, which is its ability to handle non-stationary data.
2. The use of cross-wavelet analysis in the development of short-term river flood forecasting models was shown to be useful, assuming there is a relatively stable phase shift between the flow and meteorological time series. Cross-wavelet analysis was used to find phase differences between flow and meteorological data and to develop cross-wavelet constituent components, both of which improved the forecasting ability of the wavelet based flood forecasting models.
3. The use of wavelet decomposed meteorological data, in addition to wavelet decomposed flow data, was shown to be useful in the development of models for short-term river flood forecasting. In order to be able to use the wavelet decomposed meteorological data for flood forecasting, a calibration constant was developed in this study and its usefulness was demonstrated in linking specific wavelengths of flow and meteorological cycles.
4. The use of a modified version of the inverse Fourier transform with a calibration constant and an edge effect correction for short-term river flood forecasting was shown to be useful for the reconstruction of wavelet and cross-wavelet derived constituent components. In order to reconstruct wavelet decomposed signals, the inverse Fourier transform can be used. However, in order to allow for a more precise reconstruction, an edge effect correction and a calibration constant for meteorological signals was applied to the inverse Fourier transform in this study.

The development of a stand-alone data-based flood forecasting method based on wavelet and cross-wavelet constituent components, with the above mentioned original contributions not found in the literature, was the main contribution of this research.

For future studies, it would be worthwhile to explore the issue of uncertainty. The two main sources of uncertainty affecting the wavelet method are measurement uncertainty and model uncertainty. For measurement uncertainty, it would be useful to explore combining gauge, satellite, and radar precipitation measurements via Bayesian model averaging. For model uncertainty, it would be useful to explore ways to improve the calibration of the models (to decrease parameter uncertainty), and ways to improve the actual structure of the model itself (to decrease structural uncertainty). Also, in order to decrease overall uncertainty with the use of wavelet models, it would be useful to explore: (i) combining the wavelet model forecasts and physically based model forecasts via simple averaging of the model forecasts; (ii) real-time updating; and iii) post-processing of the model flood forecast via bias correction, Bayesian model averaging, or Bayesian processor of ensemble (BPE).

To summarize, two main conclusions can be derived from the results of this study:

1. It was found that flood forecasting models based on wavelet and cross-wavelet constituent components can be successfully used for short-term 1 and 3 days lead time flood forecasting.
2. In the case of 7 days lead time flood forecasting, models based on wavelet and cross-wavelet constituent components were found to be less accurate, with ANN models providing more accurate results.

ACKNOWLEDGEMENTS

The author would like to thank his supervisor Professor Janusz Kindler of the Institute of Environmental Engineering Systems at the Warsaw University of Technology for his very valuable advice throughout the course of this research. Comments provided by Professor Marek Nawalany of the Institute of Environmental Engineering Systems at the Warsaw University of Technology, and Professor Jaroslaw Napiorkowski of the Institute of Geophysics at the Polish Academy of Sciences, are also appreciated

REFERENCES

Appenzeller C, Stocker TF, Anklin M. 1998. North Atlantic oscillation dynamics recorded in Greenland ice cores. *Science* **282**: 446–449.

Cannas B, Fanni A, Sias G, Tronei S, Zedda MK. 2005. River flow forecasting using neural networks and wavelet analysis. *Proceedings of the European Geosciences Union*, 31 August; 12–21.

Coulibaly P, Anctil F, Bobee B. 2000. Daily reservoir inflow forecasting using artificial neural networks with stopped training approach. *Journal of Hydrology* **230**: 244–257.

Gedalof Z, Smith DJ. 2001. Interdecadal climate variability and regime–scale shifts in Pacific North America. *Geophysical Research Letters* **28**: 1515–1518.

Hsu K, Gupta HV, Sorooshian S. 1995. Artificial neural network modeling of rainfall–runoff process. *Water Resources Research* **31**: 2517–2530.

Hudgins L, Friehe CA, Mayer ME. 1993. Wavelet transforms and atmospheric turbulence. *APS Physical Review* **71**: 3279–3282.

Jury MR, Enfield DB, Melice JL. 2002. Tropical monsoons around Africa: stability of El Nino–southern oscillation associations and links with continental climate. *Journal of Geophysical Research* **107**.

Kang KW, Kim JH, Park CY, Ham KJ. 1993. Evaluation of hydrological forecasting system based on neural network model. In *Proceedings of the 25th Congress of the International Association for Hydraulic Research*, Delft, Netherlands; 257–264.

Kim G, Barros AP. 2001. Quantitative flood forecasting using multisensor data and neural networks. *Journal of Hydrology* **246**: 45–62.

Kim TW, Valdes JB. 2003. A nonlinear model for drought forecasting based on conjunction of wavelet transforms and neural networks. *Journal of Hydrologic Engineering* **8**: 319–328.

Labat D, Ababou R, Mangin A. 1999. Wavelet analysis in Karstic hydrology. 2nd Part: Rainfall–runoff cross–wavelet analysis. *Comptes Rendus de l'Academie des Sciences Series IIA Earth and Planetary Science* **329**: 881–887.

Lane SN. 2007. Assessment of rainfall–runoff models based upon wavelet analysis. *Hydrological Processes* **21**: 586–607.

Morlet J, Arens G, Fourgeau I, Giard D. 1982. Wave propagation and sampling theory. *Geophysics* **47**: 203–236.

Nash JE, Sutcliffe JV. 1970. River flow forecasting through conceptual models. I. A discussion of principles. *Journal of Hydrology* **10**: 282–290.

Nayak PC, Sudheer KP, Rangan DM, Ramasastni KS. 2005. Short–term flood forecasting with a neurofuzzy model. *Water Resources Research* **41**: 1–16.

Piotrkowski A, Napiorkowski JJ, Rowinski PM. 2006. Flashflood forecasting by means of neural networks and nearest neighbour approach—a comparative study. *Nonlinear Processes in Geophysics* **13**: 443–338.

Prokoph A. 2006. XCWT.F cross–wavelet software program. Unpublished.

Prokoph A, Barthelmes F. 1996. Detection of nonstationarities in geological time series: wavelet transform of chaotic and cyclic sequences. *Computers and Geosciences* **10**: 1097–1108.

Saco P, Kumar P. 2000. Coherent modes in multiscale variability of streamflow over the United States. *Water Resources Research* **36**: 1049–1068.

Smith LC, Turcotte DL, Isacks BL. 1998. Stream flow characterization and feature detection using a discrete wavelet transform. *Hydrological Processes* **12**: 233–249.

Tantanee S, Patamatammakul S, Oki T, Sriboonlue V, Prempree T. 2005. Coupled wavelet–autoregressive model for annual rainfall prediction. *Journal of Environmental Hydrology* **13**.

Tawfik M. 2003. Linearity versus non–linearity in forecasting Nile River flows. *Advances in Engineering Software* **34**: 515–524.

Torrence C, Compo G. 1998. A practical guide to wavelet analysis. *Bulletin of the American Meteorological Society* **79**: 61–78.

Torrence C, Webster PJ. 1999. Interdecadal changes in the ENSO–Monsoon System. *Journal of Climatology* **12**: 2679–2690.

Wang R, Lee T. 1998. A study on the wavelet model of upland watersheds and its application to hydrological estimation. *Proceedings of Statistical Methods for Hydrologic Systems*. **7**: 08651.

DOI: 10.1002/hyp